

Structure of Superheavy Nuclei Along Element 115 Decay Chains

Yue Shi (石跃),^{1,2} D.E. Ward,³ B.G. Carlsson,³ J. Dobaczewski,^{4,5}

W. Nazarewicz,^{1,6,4} I. Ragnarsson,³ and D. Rudolph⁷

¹*Department of Physics and Astronomy, University of Tennessee, Knoxville, Tennessee 37996, USA*

²*Joint Institute for Heavy Ion Research, Oak Ridge National Laboratory, Oak Ridge, Tennessee 37831, USA*

³*Division of Mathematical Physics, LTH, Lund University, SE-22100, Lund, Sweden*

⁴*Institute of Theoretical Physics, Faculty of Physics,*

University of Warsaw, ul. Hoża 69, PL-00681 Warsaw, Poland

⁵*Department of Physics, PO Box 35 (YFL), FI-40014 University of Jyväskylä, Finland*

⁶*Physics Division, Oak Ridge National Laboratory, Oak Ridge, Tennessee 37831, USA*

⁷*Department of Physics, Lund University, SE-22100, Lund, Sweden*

A recent high-resolution α , X-ray, and γ -ray coincidence-spectroscopy experiment offered a first glimpse of excitation schemes of isotopes along α -decay chains of $Z = 115$. To understand these observations and to make predictions about shell structure of superheavy nuclei below $^{288}115$, we employ two complementary mean-field models: self-consistent Skyrme Energy Density Functional approach and the macroscopic-microscopic Nilsson model. We discuss the spectroscopic information carried by the new data. In particular, candidates for the experimentally observed $E1$ transitions in ^{276}Mt are proposed. We find that the presence and nature of low-energy $E1$ transitions in well-deformed nuclei around $Z = 110$, $N = 168$ strongly depends on the strength of the spin-orbit coupling; hence, it provides an excellent constraint on theoretical models of superheavy nuclei. To clarify competing theoretical scenarios, an experimental search for $E1$ transitions in odd- A systems $^{275,277}\text{Mt}$, ^{275}Hs , and ^{277}Ds is strongly recommended.

PACS numbers: 21.60.Jz, 21.10.-k, 23.20.Lv, 23.60.+e, 27.90.+b

I. INTRODUCTION

Superheavy nuclei at the limit of nuclear mass and atomic number pose a formidable challenge to both experiment and theory. The low cross sections for production of these nuclei, in the picobarn range or less, offer limited structural information. Moreover, the α -decay chains of nuclei synthesized in experiments using a ^{48}Ca beam with actinide targets [1–9] terminate by spontaneous fission before reaching the known region of the nuclear chart. This poses a problem with the unambiguous identification of the new isotopes, and more direct techniques to determine Z and A must be employed [9]. Theoretical predictions of the shell structure of superheavy nuclei are also difficult, as the interplay between the electrostatic repulsion and nuclear attraction, combined with a very high density of single-particle (s.p.) states, make the results of calculations extremely sensitive to model details [10–15].

In a recent experimental study [9, 16], unique structural information on low-lying states in superheavy nuclei below $^{288}115$ has been obtained. Of particular interest is the finding that some of the measured transitions in the nucleus assigned to be ^{276}Mt have $E1$ character, thus suggesting opposite parities of the connected states. The new data offer an exciting opportunity to constraint theoretical models in this region for the first time. Indeed, previous macroscopic-microscopic [17–19] and self-consistent studies [20, 21] have shown that the number of opposite-parity s.p. orbitals around the Fermi level is fairly limited, and this is consistent with the Nilsson model analysis of Ref. [9].

Because of the above-mentioned sensitivity to model details, robust predictions in this region are difficult to make as one is dealing with large extrapolations. To this end, when aiming at reliable predictions, it is advisable to use a model that performs well in the neighboring region where experimental information is more abundant. Furthermore, since the quadrupole deformations of α -decay daughters of $^{288}115$ are expected to increase gradually with decreasing Z and A along the α -decay chain [13, 14, 17–21], shape polarization is going to play a role when determining the energies of low-lying states.

In this work, we study the low-lying states in the superheavy nuclei below $^{288}115$, using the locally-optimized self-consistent Skyrme Energy Density Functional (SEDF) and Nilsson-Strutinsky (NS) frameworks. To assess the robustness of these results, we also carry out calculations using a globally-optimized SEDF model.

II. MODELS

The SEDF approach is a variant of nuclear density functional theory, which offers a global, self-consistent description of nuclear properties across the nuclear landscape [22, 23]. The recent self-consistent study of Ref. [15] offers a locally optimized SEDF parameterization UNEDF1^{SO} that meets our local-extrapolability requirements: it reproduces one-quasiparticle (1-q.p.) states in ^{251}Cf and ^{249}Bk (the two heaviest systems where 1-q.p. energies are experimentally well known), predicts crucial deformed shell gaps at $N = 152$ and $Z = 100$, and describes rotational bands in Fm, No, and Rf iso-

topes. The parameter set UNEDF1^{SO} has been obtained by adjusting the spin-orbit coupling constants of a global SEDF parametrization UNEDF1 [24] that performs well for heavy nuclei and large deformations. We shall also use UNEDF1 in this study. The calculations follow closely Ref. [15]. The Skyrme Hartree-Fock-Bogolyubov (SHFB) equations were solved using the symmetry-unrestricted solver HFODD (v2.52j) [25] by expanding 1-q.p. wave functions in 680 deformed harmonic-oscillator (HO) basis states. To compute 1-q.p. excitations in odd- A nuclei, we blocked relevant orbits around the Fermi level as described in Ref. [26]. The strengths of the pairing force for neutrons and protons were adjusted to the odd-even mass staggering in ^{251}Cf and ^{249}Bk and the kinematic moment of inertia of ^{252}No .

The SEDF results are compared with those of the Nilsson-Strutinsky (NS) approach of Ref. [27] with the modified harmonic oscillator (MO) potential and pairing as in Ref. [28]. The shell-independent MO parameters ($\kappa_p = 0.058$, $\mu_p = 0.63$, $\kappa_n = 0.0526$, and $\mu_n = 0.457$) have been locally optimized to the actinide nuclei [29] and applied to, e.g., $^{228,230}\text{Pa}$ [30] and ^{242}Am [31].

The 2-q.p.-plus-rotor calculations for odd-odd nuclei were carried out using the MO model of Ref. [32]. The moments of inertia were chosen according to a phenomenological relation of Ref. [33]. The BCS pairing was treated as in Ref. [28], with the monopole pairing strengths taken as 95% of the values for even-even nuclei. No residual proton-neutron interaction was considered.

III. RESULTS

We first discuss properties of the even-even nuclei belonging to the α -decay chain of $^{296}120$. Their ground states form q.p. vacua for neighboring odd- A and odd-odd systems. The calculated quadrupole moments are shown in Fig. 1. Both SEDF models predict a similar smooth increase of quadrupole deformation along the α -chain. In the NS calculations, $^{296}120$ is nearly spherical, $^{292}118$ and ^{288}Lv are very weakly deformed, ^{284}Fl and ^{280}Cn are spherical, and the shapes of the lightest daughters have deformations close to those predicted by SEDF. These results suggest that a direct comparison between SEDF and NS models is most meaningful for $Z < 112$.

It is instructive to begin the discussion from the Nilsson s.p. diagram of the MO potential shown in Fig. 2. The main features of this diagram, such as the appearance of spherical shell gaps at $Z = 114$ and $N = 184$, have remained unchanged since the late 1960s [35, 36]. It is worth noting that the s.p. spectrum of the MO model, with its pronounced spherical shell gaps at $Z = 114$ and $N = 184$ and resulting Nilsson orbits, is fairly close to that of more realistic Woods-Saxon [17–19] and Folded-Yukawa [37–39] potentials, see Refs. [10, 40] for more discussion.

The deformed shell structure of nuclei at the end of the α -decay chain of $^{296}120$ (or $^{288}115$) is relatively simple:

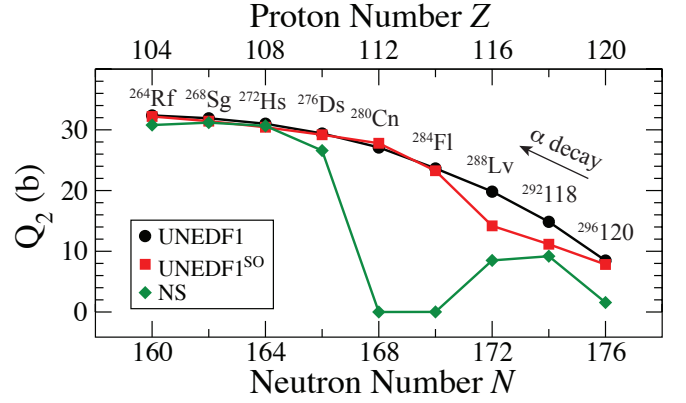


FIG. 1. (Color online) Quadrupole moments Q_2 of even-even nuclei forming the α -decay chain $^{296}120 \rightarrow \dots \rightarrow ^{264}\text{Rf}$, calculated with UNEDF1^{SO} and UNEDF1 SEDF models and the NS approach.

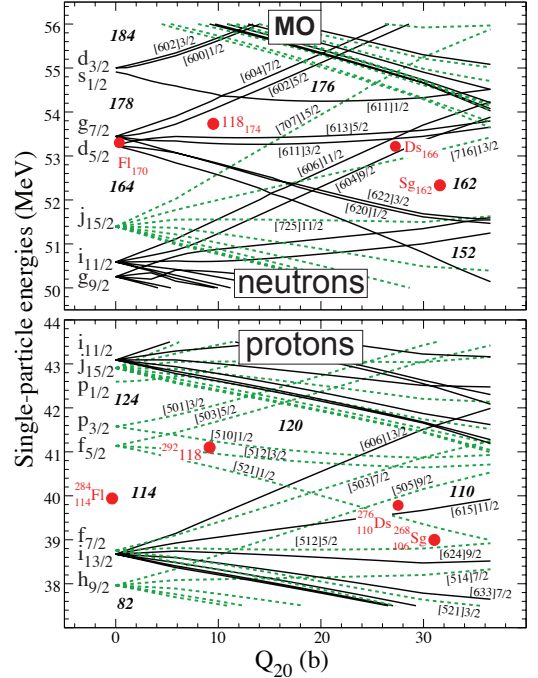


FIG. 2. (Color online) Nilsson diagram for neutrons (top) and protons (bottom) for nuclei along the α -decay chain of $^{296}120$ using the MO potential of Ref. [29]. The orbits are labelled by the standard asymptotic Nilsson numbers [28]. The positive/negative parity levels are marked by solid/dashed lines. The Fermi levels of nuclei in Fig. 1 are indicated by dots. The quadrupole moment was determined from shape deformations ϵ_2 and ϵ_4 [34]: $Q_{20} = 0.8AR_0^2(\epsilon_2 + 0.5\epsilon_2^2 + 0.758\epsilon_4^2 - \epsilon_2\epsilon_4)$ with $A = 280$, $R_0 = r_0A^{1/3}$, and $r_0 = 1.217$ fm.

both in neutrons and protons there appears one unique-parity, high- Ω Nilsson state ($\nu[716]13/2$ and $\pi[615]11/2$) surrounded by levels of opposite parity, such as neutron ($[613]5/2$, $[611]3/2$), ($[606]11/2$, $[604]9/2$) and proton ($[503]7/2$, $[505]9/2$), ($[510]1/2$, $[512]3/2$) pseudo-spin doublets, respectively.

The spherical shell structure in superheavy nuclei strongly depends on the spin-orbit splitting, which governs the size of the $Z = 114$ gap (cf. Table 4 of Ref. [10] and discussion therein). Also, the coupling between Coulomb interaction and nuclear interaction is expected to impact the predictions. To consider both effects, we studied s.p. canonical states obtained with UNEDF1^{SO} and UNEDF1 SEDF models, which differ in the spin-orbit sector and treat the electrostatic energy self-consistently.

The s.p. energies of UNEDF1^{SO} along the α -decay chain of $^{296}120$ are depicted in Fig. 3.

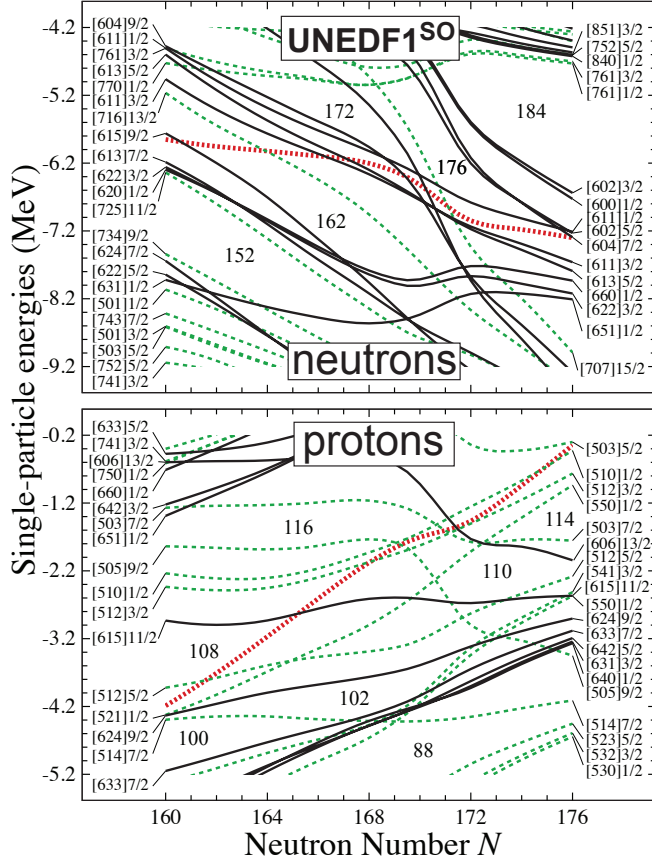


FIG. 3. (Color online) Single-neutron (top) and single-proton (bottom) canonical energies of UNEDF1^{SO} for nuclei along the α -decay chain of $^{296}120$ as in Fig. 1. The orbits are labelled by the standard asymptotic Nilsson numbers corresponding to the dominant components of the SHFB canonical wave functions. The positive/negative parity levels are marked by solid/dashed lines. The Fermi levels are indicated by thick dotted lines.

The s.p. neutron spectrum is dominated by deformed gaps at $N = 152$ and 162 , and a large spherical shell gap at $N = 184$. In the deformed region $160 \leq N \leq 168$, the Nilsson states close to the Fermi level are primarily $N_{\text{osc}} = 6$ levels and one unique-parity, high- Ω intruder level $\nu[716]13/2$ originating from the spherical $1j_{15/2}$ shell. The structure of the proton Nilsson diagram in Fig. 3 is dominated by deformed gaps at $Z = 100, 102$,

and 108 , and a spherical subshell closure at $Z = 114$. The unique-parity, high- Ω intruder level $\pi[615]11/2$ originating from the spherical $1i_{13/2}$ shell is surrounded by several $N_{\text{osc}} = 5$ Nilsson orbitals.

The general pattern of s.p. states predicted by UNEDF1^{SO} is not that far from that in Fig. 2 of the MO potential. However, there are differences in the spherical shell structure, which will impact detailed predictions for deformed superheavy nuclei belonging to $Z = 115$ α -decay chains. In particular, MO predicts larger spherical shell gaps at $Z = 114$, $N = 148$, and $N = 178$. In UNEDF1^{SO}, the splitting between the $1j_{15/2}$ and $1i_{11/2}$ spherical neutron shells is very small. This results in an upward shift of the $([606]11/2, [604]9/2)$ doublet.

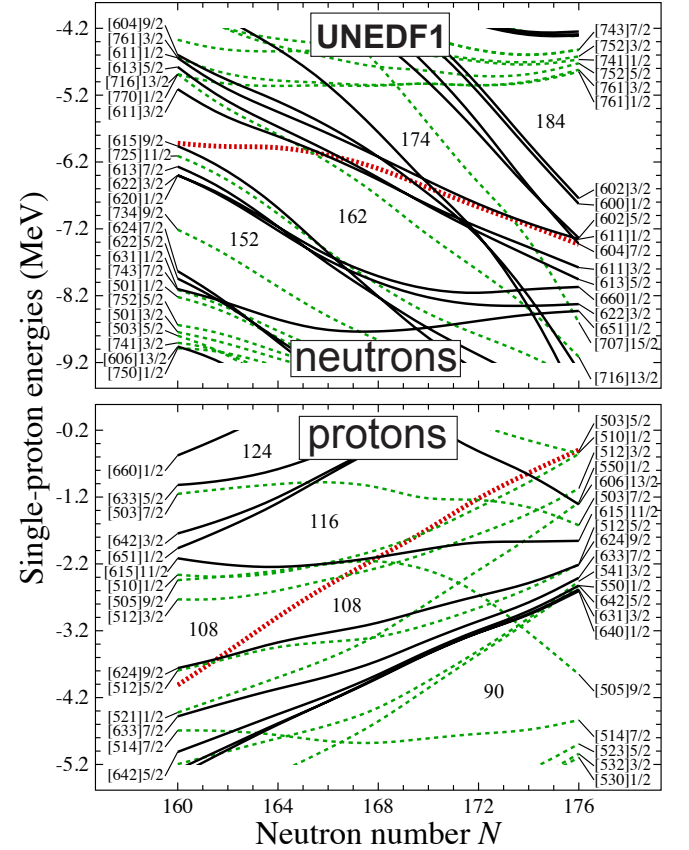


FIG. 4. (Color online) Similar as in Fig. 3 but for UNEDF1

As seen in Fig. 4, in the case of UNEDF1 the unique-parity $\nu 1j_{15/2}$ and $\pi 1i_{13/2}$ shells are shifted up by a few hundred keV, which results in a significant reduction of spherical $N = 164$ and $Z = 114$ shell closures [15]. The change in the spin-orbit potential also impacts positions of deformed levels. In particular, the deformed neutron gap at $N = 152$ is reduced, and that at $N = 162$ opens up. In the proton sector, the deformed Nilsson state $[615]11/2$ appears just below the significantly increased $Z = 116$ gap, close to the $[505]9/2$ and $[510]1/2$ levels. The second proton intruder state $[624]9/2$ shows up just below the deformed proton gap at $Z = 108$.

A. One-quasi-particle energies

To get more insights, we computed the energies of 1-q.p. excitations for odd- Z , even- N superheavy nuclei that form the α -decay chains of $^{287}_{116}\text{Lv}_{171}$ and $^{289}_{116}\text{Lv}_{173}$ (Tables I and II), and $^{287}_{115}\text{Lv}_{172}$ and $^{293}_{117}\text{Lv}_{176}$ (Tables III and IV); the theoretical error on 1-q.p. excitations due to the adopted size of the HO basis is less than 60 keV when going from 680 stretched HO states to 969 states. The results for $^{287}_{116}\text{Lv}_{171}$ and $^{293}_{117}\text{Lv}_{176}$ are shown in Figs. 5 and 6, respectively.

TABLE I. Excitation energies, total quadrupole moments, and quadrupole mass deformations β_2 for one-quasi-particle excitations in selected nuclei belonging to the α -decay chains of $^{287,289}\text{Lv}$ predicted with UNEDF1^{SO}. The high- Ω unique-parity states are printed in boldface. The intrinsic configurations are labelled as in Fig. 3. The predictions on the lightest member of ^{289}Lv α -decay chain, ^{277}Ds , are discussed below.

Nucleus	Config.	E_x (MeV)	Q_{20} (b)	β_2
$^{275}_{110}\text{Ds}_{165}$	[613]5/2	0	29.8	0.23
	[613]3/2	0.085	29.7	0.23
	[716]13/2	0.151	29.9	0.23
	[611]1/2	0.305	29.8	0.23
	[604]9/2	0.619	29.4	0.22
$^{279}_{112}\text{Cn}_{167}$	[611]3/2	0	28.3	0.21
	[613]5/2	0.013	28.3	0.21
	[611]1/2	0.121	28.3	0.21
	[604]9/2	0.306	28.0	0.21
	[716]13/2	0.627	28.5	0.22
$^{281}_{112}\text{Cn}_{169}$	[611]1/2	0	27.2	0.20
	[604]9/2	0.145	27.4	0.21
	[613]5/2	0.159	27.1	0.20
	[611]3/2	0.237	26.2	0.20
	[606]11/2	0.606	24.8	0.19
$^{283}_{114}\text{Fl}_{169}$	[611]1/2	0	25.4	0.19
	[604]9/2	0.165	25.0	0.19
	[613]5/2	0.184	24.9	0.19
	[611]3/2	0.208	24.5	0.18
	[606]11/2	0.399	23.6	0.18
$^{285}_{114}\text{Fl}_{171}$	[611]1/2	0	21.0	0.15
	[613]5/2	0.051	19.0	0.14
	[611]3/2	0.056	19.0	0.14
	[606]11/2	0.058	21.0	0.15
	[707]15/2	0.232	19.6	0.14
$^{287}_{116}\text{Lv}_{171}$	[613]5/2	0	14.2	0.10
	[611]3/2	0.085	14.2	0.10
	[707]15/2	0.219	14.8	0.10
	[611]1/2	0.314	14.3	0.10
	[622]3/2	0.378	13.1	0.09
	[604]9/2	0.495	16.2	0.12
$^{289}_{116}\text{Lv}_{173}$	[613]5/2	0	11.8	0.08
	[611]3/2	0.029	11.8	0.08
	[611]1/2	0.055	11.9	0.08
	[604]7/2	0.372	11.2	0.08
	[602]5/2	0.397	11.3	0.08

Although s.p. energies are not experimental observ-

ables, those around the Fermi level carry information about the low-lying q.p. configurations in neighboring odd- A and odd-odd nuclei.

TABLE II. Similar as in Table I but for UNEDF1.

Nucleus	Config.	E_x (MeV)	Q_{20} (b)	β_2
$^{275}_{110}\text{Ds}_{165}$	[613]5/2	0	30.2	0.23
	[611]3/2	0.050	30.2	0.23
	[716]13/2	0.121	30.2	0.23
	[611]1/2	0.364	30.2	0.23
	[604]9/2	0.561	29.8	0.23
$^{279}_{112}\text{Cn}_{167}$	[611]3/2	0	28.1	0.21
	[613]5/2	0.044	28.1	0.21
	[611]1/2	0.074	28.2	0.21
	[716]13/2	0.197	28.3	0.21
	[604]9/2	0.201	27.8	0.21
$^{281}_{112}\text{Cn}_{169}$	[611]1/2	0	26.3	0.19
	[604]9/2	0.109	26.2	0.19
	[611]3/2	0.152	25.7	0.19
	[613]5/2	0.157	26.0	0.19
	[606]11/2	0.267	25.0	0.19
$^{283}_{114}\text{Fl}_{169}$	[611]1/2	0	25.5	0.19
	[604]9/2	0.114	25.1	0.19
	[611]3/2	0.147	24.7	0.18
	[613]5/2	0.160	24.6	0.18
	[606]11/2	0.195	24.3	0.18
$^{285}_{114}\text{Fl}_{171}$	[604]9/2	0	22.8	0.17
	[611]1/2	0.009	22.2	0.17
	[611]3/2	0.139	21.5	0.16
	[606]11/2	0.169	22.2	0.17
	[613]5/2	0.184	21.4	0.16
$^{287}_{116}\text{Lv}_{171}$	[707]15/2	0.723	20.4	0.15
	[604]9/2	0	21.8	0.16
	[611]1/2	0.003	21.2	0.15
	[611]3/2	0.113	20.5	0.15
	[613]5/2	0.175	20.4	0.15
$^{289}_{116}\text{Lv}_{173}$	[606]11/2	0.204	21.2	0.15
	[707]15/2	0.661	19.2	0.14
	[611]1/2	0	18.1	0.13
	[611]3/2	0.256	17.7	0.13
	[613]5/2	0.394	17.8	0.13
$^{289}_{116}\text{Lv}_{173}$	[604]9/2	0.649	18.4	0.13
	[707]15/2	0.796	18.0	0.13

B. Odd-odd nuclei

By combining the low-lying 1-q.p. excitations, one can deduce possible 2-q.p. states in the odd-odd nuclei that form α -decay chains of $^{288}\text{115}$. It is worth noting that there exist detailed calculations of 1-q.p. excitations in the heaviest elements using the macroscopic-microscopic Woods-Saxon model [17–19]; unfortunately, they cannot be used to assess the neutron s.p. structure in the region of interest as the range of neutron numbers covered ($N \leq 161$) in these papers is too limited.

TABLE III. Similar as in Table I but for one-quasi-proton excitations in the α -decay chains of $^{293}\text{117}$ and $^{287}\text{115}$ predicted with UNEDF1^{SO}.

Nucleus	Config.	E_x (MeV)	Q_{20} (b)	β_2
$^{279}_{111}\text{Rg}_{168}$	[512]3/2	0	28.3	0.21
	[510]1/2	0.122	28.3	0.21
	[615]11/2	0.284	28.4	0.21
	[505]9/2	0.392	27.7	0.20
	[521]1/2	0.633	26.6	0.19
$^{281}_{111}\text{Rg}_{170}$	[512]3/2	0	26.0	0.20
	[510]1/2	0.165	26.1	0.20
	[505]9/2	0.263	25.8	0.20
	[615]11/2	0.277	26.1	0.20
	[521]1/2	0.412	25.3	0.19
$^{283}\text{113}_{170}$	[512]3/2	0	24.5	0.18
	[510]1/2	0.057	24.5	0.18
	[505]9/2	0.090	24.4	0.18
	[503]7/2	0.453	22.9	0.16
	[521]1/2	0.629	23.2	0.16
$^{285}\text{113}_{172}$	[512]3/2	0	18.7	0.14
	[503]7/2	0.096	17.6	0.13
	[550]1/2	0.146	17.2	0.13
	[510]1/2	0.177	19.4	0.15
	[505]9/2	0.380	19.7	0.15
$^{287}\text{115}_{172}$	[615]11/2	0.645	18.2	0.14
	[512]3/2	0	14.4	0.10
	[550]1/2	0.042	12.6	0.09
	[503]7/2	0.127	14.2	0.10
	[606]13/2	0.206	14.2	0.10
$^{289}\text{115}_{174}$	[510]1/2	0.388	14.1	0.10
	[550]1/2	0	11.3	0.08
	[512]3/2	0.002	11.5	0.08
	[606]13/2	0.137	12.2	0.09
	[503]7/2	0.230	11.6	0.08
$^{293}\text{117}_{176}$	[510]1/2	0.338	11.6	0.08
	[512]3/2	0	7.8	0.05
	[550]1/2	0.06	7.5	0.05
	[510]1/2	0.218	7.8	0.05
	[503]5/2	0.310	7.0	0.04
$^{293}\text{117}_{176}$	[503]7/2	0.778	8.1	0.06

Let us look into the structure of ^{276}Mt in some detail. The structural information relevant to this nucleus is contained in the 1-q.p. spectra of its odd- A neighbors $^{275,277}\text{Mt}$, ^{275}Hs , and ^{277}Ds , provided in SEDF Table V. All low-lying 1-q.p. states in these nuclei correspond to very similar quadrupole mass deformation of $\beta_2 \approx 0.22$, which facilitates comparison with the Nilsson diagram of Fig. 3. The lowest 1-q.p. proton states are the unique-parity [615]11/2 and $N_{\text{osc}} = 5$ excitations [512]3/2, [521]1/2, [510]1/2, and [512]5/2. The 1-q.p. neutron structure corresponds to the [716]13/2 intruder and $N_{\text{osc}} = 6$ [611]3/2, [613]5/2, [611]1/2, and [604]9/2 Nilsson orbits. The most significant difference between the two SEDF models is the appearance of the [505]9/2 1-q.p. proton excitation low in energy in UNEDF1. According to the MO model of Fig. 2, the low-

TABLE IV. Similar as in Table III but with UNEDF1.

Nucleus	Config.	E_x (MeV)	Q_{20} (b)	β_2
$^{279}_{111}\text{Rg}_{168}$	[512]3/2	0	27.8	0.21
	[615]11/2	0.075	27.8	0.21
	[505]9/2	0.119	27.6	0.21
	[510]1/2	0.252	27.8	0.21
	[624]9/2	0.793	27.6	0.21
$^{281}_{111}\text{Rg}_{170}$	[615]11/2	0	25.3	0.19
	[512]3/2	0.021	25.3	0.19
	[505]9/2	0.087	25.4	0.19
	[510]1/2	0.218	25.3	0.19
	[521]1/2	0.601	23.9	0.18
$^{283}\text{113}_{170}$	[510]1/2	0	24.3	0.18
	[512]3/2	0.024	24.1	0.18
	[615]11/2	0.055	24.3	0.18
	[503]7/2	0.480	22.7	0.17
	[550]1/2	0.702	22.7	0.17
$^{285}\text{113}_{172}$	[510]1/2	0	21.2	0.16
	[512]3/2	0.044	21.0	0.15
	[615]11/2	0.089	21.1	0.15
	[505]9/2	0.287	22.8	0.16
	[550]1/2	0.411	19.8	0.15
$^{287}\text{115}_{172}$	[510]1/2	0	20.2	0.15
	[503]7/2	0.055	20.1	0.15
	[512]3/2	0.193	20.1	0.15
	[615]11/2	0.253	20.4	0.15
	[550]1/2	0.682	19.1	0.14
$^{289}\text{115}_{174}$	[503]7/2	0	17.1	0.12
	[512]3/2	0.024	16.9	0.12
	[510]1/2	0.085	17.1	0.12
	[615]11/2	0.272	17.3	0.12
	[550]1/2	0.438	16.5	0.12
$^{293}\text{117}_{176}$	[510]1/2	0	11.4	0.08
	[606]13/2	0.003	11.5	0.08
	[512]3/2	0.03	11.2	0.08
	[550]1/2	0.197	9.7	0.06
	[503]5/2	0.26	11.1	0.08
$^{293}\text{117}_{176}$	[503]7/2	0.266	11.7	0.08
	[615]11/2	0.588	11.4	0.08

est 1-q.p. proton excitations are the [615]11/2, [521]1/2, and [505]9/2 Nilsson orbits, while the lowest neutron states are: [606]11/2, [604]9/2, [611]3/2, [613]5/2, and [716]13/2. It is interesting to note that the structure of 1-q.p. proton states predicted for ^{275}Mt in Ref. [18] falls between predictions of UNEDF1 and UNEDF1^{SO}. In addition, within the Woods-Saxon model of Ref. [41], the proton states [615]11/2 and [505]9/2 are the two lowest orbitals for Mt over a large range of deformations.

As noted in [9], there is a very limited choice of q.p. configurations that could generate the observed $E1$ transitions in ^{276}Mt . If one insists on a strict conservation of the Ω quantum number for protons and neutrons, no low-energy $E1$ transitions are predicted by UNEDF1^{SO}. Formally, one can construct states that can be connected by an $\Delta\Omega = 0, \pm 1$, parity changing operator, e.g., $\{\pi[615]11/2 \otimes \nu[613]5/2\}_{3+}$ and $\{\pi[521]1/2 \otimes$

TABLE V. Similar as in Table I but for one-quasi-particle excitations in the odd- A neighbors of $^{276}\text{Mt}_{167}$ predicted with UNEDF1^{SO} and UNEDF1.

Nucleus	Config.	E_x (MeV)	Q_{20} (b)	β_2
UNEDF1 ^{SO}				
$^{275}\text{Mt}_{166}$	[615]11/2	0	29.7	0.23
	[512]3/2	0.243	29.5	0.23
	[521]1/2	0.402	29.2	0.22
	[512]5/2	0.500	29.7	0.23
	[510]1/2	0.512	29.7	0.23
$^{277}\text{Mt}_{168}$	[615]11/2	0	28.3	0.23
	[521]1/2	0.174	27.4	0.21
	[512]3/2	0.269	28.3	0.23
	[510]1/2	0.480	28.3	0.23
	[512]5/2	0.532	28.3	0.23
$^{275}\text{Hs}_{167}$	[613]5/2	0	28.9	0.22
	[611]3/2	0.016	28.9	0.22
	[611]1/2	0.117	28.9	0.22
	[604]9/2	0.235	28.2	0.22
	[716]13/2	0.479	29.4	0.23
$^{277}\text{Ds}_{167}$	[611]3/2	0	28.6	0.22
	[613]5/2	0.046	28.9	0.22
	[611]1/2	0.107	28.7	0.22
	[604]9/2	0.335	28.6	0.22
	[716]13/2	0.564	29.2	0.22
UNEDF1				
$^{275}\text{Mt}_{166}$	[512]3/2	0	30.0	0.23
	[615]11/2	0.159	29.6	0.23
	[505]9/2	0.167	29.0	0.22
	[510]1/2	0.173	30.1	0.23
	[624]9/2	0.318	29.9	0.23
$^{277}\text{Mt}_{168}$	[512]3/2	0	28.6	0.22
	[615]11/2	0.131	28.2	0.21
	[505]9/2	0.136	27.5	0.21
	[512]5/2	0.182	28.6	0.22
	[624]9/2	0.300	28.5	0.21
$^{275}\text{Hs}_{167}$	[613]5/2	0	29.4	0.22
	[611]3/2	0.067	29.4	0.22
	[611]1/2	0.104	29.5	0.22
	[716]13/2	0.173	29.7	0.23
	[604]9/2	0.242	29.1	0.22
$^{277}\text{Ds}_{167}$	[611]3/2	0	28.9	0.22
	[613]5/2	0.035	29.0	0.22
	[611]1/2	0.090	29.0	0.22
	[716]13/2	0.157	29.2	0.22
	[604]9/2	0.227	28.7	0.22

mentally, this calls for high-resolution α -photon coincidence spectroscopy of decay chains starting from $^{293}\text{117}$, $^{287,289}\text{115}$, or $^{285,287}\text{Fl}$, respectively. However, the observation of these systems is hampered either by relatively low production cross-sections or large spontaneous fission branches on the way to the nuclei of structural interest [1–9]. A solution to this spectroscopic puzzle may significantly contribute to our understanding of shell structure in superheavy nuclei, and the strength of the spin-orbit splitting in particular.

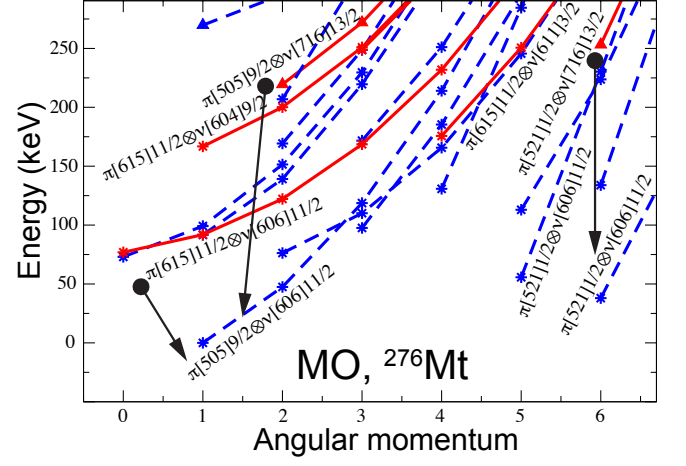


FIG. 7. (Color online) Results of 2-q.p.-plus-rotor NS calculations for ^{276}Mt . States connected with lines have the same dominating single-particle configurations; they can be interpreted as rotational bands built on 2-q.p. bandheads indicated. Solid/dashed lines mark bands with positive/negative parity. Positive/negative parity neutron configurations are indicated by asterisks/triangles. The candidates for stretched $\Delta\Omega = 0, \pm 1$ E1 transitions are marked by thick arrows.

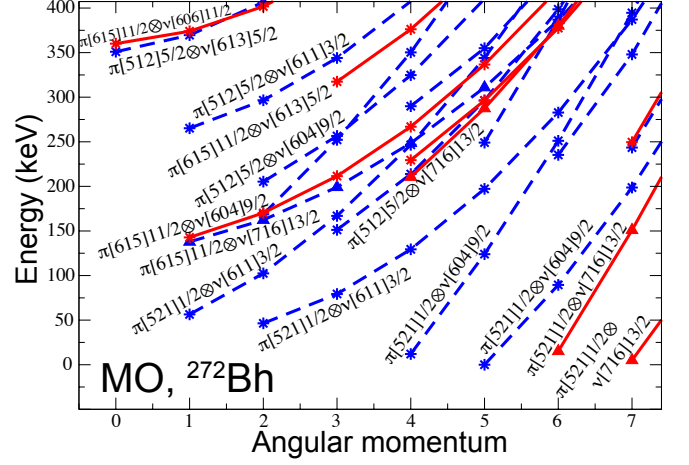


FIG. 8. (Color online) Similar as in Fig. 7 but for ^{272}Bh .

ACKNOWLEDGMENTS

Discussions with S. Åberg are gratefully acknowledged. This work was supported by the U.S. Department of Energy (DOE) under Contracts No. DE-FG02-96ER40963 (University of Tennessee), No. de-sc0008499 (NUCLEI SciDAC Collaboration), No. de-na0001820 (the Stewardship Science Academic Alliances program); by the Academy of Finland and University of Jyväskylä within the FIDIPRO programme; by the Polish National Science Center under Contract No. 2012/07/B/ST2/03907; and by the Swedish Research Council. An award of computer time was provided by the National Institute for Computational Sciences (NICS) and the Innovative and

TABLE VI. Similar as in Table V but for one-quasi-particle excitations in the odd- A neighbors of $^{272}\text{Bh}_{165}$ predicted with UNEDF1^{SO} and UNEDF1.

Nucleus	Config.	E_x (MeV)	Q_{20} (b)	β_2
UNEDF1 ^{SO}				
$^{271}\text{Bh}_{164}$	[512]5/2	0	30.8	0.24
	[521]1/2	0.076	30.3	0.23
	[615]11/2	0.244	30.4	0.23
	[624]9/2	0.415	30.8	0.24
	[514]7/2	0.682	31.1	0.24
$^{273}\text{Bh}_{166}$	[615]11/2	0	29.3	0.23
	[512]5/2	0.002	29.6	0.23
	[521]1/2	0.072	29.5	0.23
	[624]9/2	0.243	29.6	0.23
	[512]3/2	0.574	29.4	0.23
$^{271}\text{Sg}_{165}$	[514]7/2	0.692	29.8	0.23
	[611]3/2	0	30.1	0.23
	[716]13/2	0.156	30.2	0.23
	[613]5/2	0.223	30.1	0.23
	[611]1/2	0.311	30.1	0.23
$^{273}\text{Hs}_{165}$	[604]9/2	0.429	29.2	0.23
	[611]3/2	0	30.1	0.23
	[613]5/2	0.118	30.0	0.23
	[716]13/2	0.142	30.3	0.23
	[611]1/2	0.314	30.1	0.23
	[604]9/2	0.518	29.2	0.22
UNEDF1				
$^{271}\text{Bh}_{164}$	[512]5/2	0	31.6	0.24
	[624]9/2	0.028	31.5	0.24
	[512]3/2	0.338	31.3	0.24
	[521]1/2	0.554	30.9	0.24
	[505]9/2	0.714	30.0	0.23
$^{273}\text{Bh}_{166}$	[624]9/2	0	30.7	0.23
	[512]5/2	0.076	30.7	0.23
	[512]3/2	0.306	30.6	0.23
	[521]1/2	0.377	29.6	0.23
	[505]9/2	0.599	28.7	0.22
$^{271}\text{Sg}_{165}$	[611]3/2	0	31.1	0.24
	[613]5/2	0.007	30.7	0.24
	[716]13/2	0.11	31.1	0.24
	[611]1/2	0.252	31.0	0.24
	[604]9/2	0.635	33.2	0.25
$^{273}\text{Hs}_{165}$	[613]5/2	0	30.7	0.24
	[611]3/2	0.048	30.8	0.24
	[716]13/2	0.119	30.8	0.24
	[611]1/2	0.300	30.8	0.24
	[604]9/2	0.508	30.4	0.23

Novel Computational Impact on Theory and Experiment (INCITE) program using resources of the OLCF facility.

-
- [1] Y. T. Oganessian, J. Phys. G **34**, R165 (2007).
 - [2] Y. T. Oganessian, Radiochim. Acta **99**, 429 (2011).
 - [3] Y. T. Oganessian *et al.*, Phys. Rev. Lett. **108**, 022502 (2012).
 - [4] Y. T. Oganessian *et al.*, Phys. Rev. Lett. **109**, 162501 (2012).
 - [5] Y. T. Oganessian *et al.*, Phys. Rev. C **87**, 014302 (2013).
 - [6] C. E. Düllmann *et al.*, Phys. Rev. Lett. **104**, 252701 (2010).
 - [7] J. M. Gates *et al.*, Phys. Rev. C **83**, 054618 (2011).
 - [8] S. Hofmann *et al.*, Eur. Phys. J. A **48**, 62 (2012).
 - [9] D. Rudolph *et al.*, Phys. Rev. Lett. **111**, 112502 (2013).
 - [10] S. Ćwiok, J. Dobaczewski, P.-H. Heenen, P. Magierski, and W. Nazarewicz, Nucl. Phys. A **611**, 211 (1996).
 - [11] A. Kruppa, M. Bender, W. Nazarewicz, P.-G. Reinhard, T. Vertse, and S. Ćwiok, Phys. Rev. C **61**, 034313 (2000).
 - [12] M. Bender, W. Nazarewicz, and P.-G. Reinhard, Phys. Lett. B **515**, 42 (2001).

- [13] S. Ćwiok, P.-H. Heenen, and W. Nazarewicz, *Nature (London)* **433**, 705 (2005).
- [14] M. Bender and P.-H. Heenen, *J. of Phys.: Conf. Ser.* **420**, 012002 (2013).
- [15] Y. Shi, J. Dobaczewski, and P. T. Greenlees, *Phys. Rev. C* **89**, 034309 (2014).
- [16] D. Rudolph *et al.*, *Acta Phys. Pol. B* **45**, 263 (2014).
- [17] S. Ćwiok, S. Hofmann, and W. Nazarewicz, *Nucl. Phys. A* **573**, 356 (1994).
- [18] A. Parkhomenko and A. Sobiczewski, *Acta Phys. Pol. B* **35**, 2447 (2004).
- [19] A. Parkhomenko and A. Sobiczewski, *Acta Phys. Pol. B* **36**, 3115 (2005).
- [20] S. Ćwiok, W. Nazarewicz, and P. H. Heenen, *Phys. Rev. Lett.* **83**, 1108 (1999).
- [21] M. Bender, *Phys. Rev. C* **61**, 031302 (2000).
- [22] M. Bender, P.-H. Heenen, and P.-G. Reinhard, *Rev. Mod. Phys.* **75** (2003).
- [23] J. Erler, N. Birge, M. Kortelainen, W. Nazarewicz, E. Olsen, A. Perhac, and M. Stoitsov, *Nature* **486**, 509 (2012).
- [24] M. Kortelainen, J. McDonnell, W. Nazarewicz, P.-G. Reinhard, J. Sarich, N. Schunck, M. V. Stoitsov, and S. M. Wild, *Phys. Rev. C* **85**, 024304 (2012).
- [25] N. Schunck, J. Dobaczewski, J. McDonnell, W. Satuła, J. Sheikh, A. Staszczak, M. Stoitsov, and P. Toivanen, *Comput. Phys. Commun.* **183**, 166 (2012).
- [26] N. Schunck, J. Dobaczewski, J. McDonnell, J. Moré, W. Nazarewicz, J. Sarich, and M. V. Stoitsov, *Phys. Rev. C* **81**, 024316 (2010).
- [27] B. G. Carlsson and I. Ragnarsson, *Phys. Rev. C* **74**, 011302 (2006).
- [28] S.G.Nilsson, C.F.Tsang, A. Sobiczewski, Z. Szymański, S. Wycech, C. Gustafson, I.-L. Lamm, P. Möller, and B. Nilsson, *Nucl. Phys. A* **131**, 1 (1969).
- [29] P. Rozmej, K. Boening, and A. Sobiczewski, in *Proceedings of XXIV Int. Winter Meeting on Nuclear Physics, Bormio, Italy*, edited by I. Iori (1986).
- [30] C. Herrmann *et al.*, *Nucl. Phys. A* **493**, 83 (1989).
- [31] A. B. Hayes *et al.*, *Phys. Rev. C* **82**, 044319 (2010).
- [32] I. Ragnarsson and P. B. Semmes, *Hyperfine Interact.* **43**, 423 (1988).
- [33] L. Grodzins, *Phys. Lett.* **2**, 88 (1962).
- [34] W. Nazarewicz and I. Ragnarsson, in *Handbook of Nuclear Properties*, ed. by D.N. Poenaru and W. Greiner, (Clarendon Press, Oxford, 1996), p. 80.
- [35] C. Gustafson, I. L. Lamm, B. Nilsson, and S. G. Nilsson, *Ark. Fys.* **36**, 613 (1967).
- [36] U. Mosel and W. Greiner, *Z. Phys.* **222**, 261 (1969).
- [37] M. Bolsterli, E. O. Fiset, J. R. Nix, and J. L. Norton, *Phys. Rev. C* **5**, 1050 (1972).
- [38] J. R. Nix, *Ann. Rev. Nucl. Sci.* **22**, 65 (1972).
- [39] P. Möller and J. Nix, *J. Phys. G* **20**, 1681 (1994).
- [40] M. Bender, K. Rutz, P.-G. Reinhard, J. Maruhn, and W. Greiner, *Phys. Rev. C* **60**, 034304 (1999).
- [41] R. R. Chasman, I. Ahmad, A. M. Friedman, and J. R. Erskine, *Rev. Mod. Phys.* **49**, 833 (1977).
- [42] V. Prassa, T. Nikšić, G. A. Lalazissis, and D. Vretenar, *Phys. Rev. C* **86**, 024317 (2012).
- [43] M. Warda and J. L. Egido, *Phys. Rev. C* **86**, 014322 (2012).
- [44] A. Staszczak, A. Baran, and W. Nazarewicz, *Phys. Rev. C* **87**, 024320 (2013).